

# Slope Disparity Gating using a Synchronized Projector-Camera System

Tomoki Ueda<sup>1</sup>, Hiroyuki Kubo<sup>1</sup>, Suren Jayasuriya<sup>2</sup>, *Member, IEEE*,  
Takuya Funatomi<sup>1</sup>, *Member, IEEE*, and Yasuhiro Mukaigawa<sup>1</sup>, *Member, IEEE*

<sup>1</sup>Nara Institute of Science and Technology, Ikoma, Japan

<sup>2</sup>Arizona State University, Tempe, AZ 85287 USA

Active illumination systems which perform disparity gating, or the ability to selectively image photons that arrive from a specified surface geometry some distance away, have recently shown usefulness for robotics, autonomous vehicles, and surveillance applications. In this paper, we present a new technique for sloped disparity gating, capturing a particular set of sloped planar surfaces in a scene, implemented using the synchronization between a raster-scanning projector and the rolling shutter of a camera. We demonstrate how to control the slope and thickness of these planar surfaces using hardware parameters of pixel clock, synchronization delay, and exposure. Finally, we perform applications including real-time image masking and imaging in scattering media with a real hardware prototype in the lab. This work showcases the potential for energy-efficient, geometry-aware disparity gating in the future.

*Index Terms*—active illumination, disparity gating, projector-camera systems, computational photography

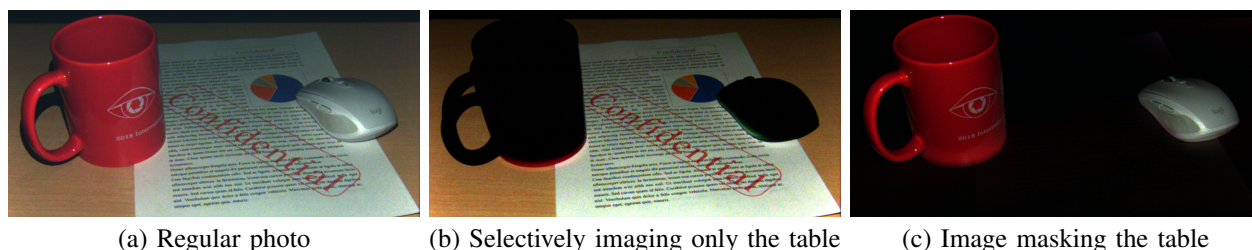


Fig. 1: Compared to a regular image (a), our imaging system can selectively image objects on a sloped plane (b), or can selectively mask objects on this plane as well (c). All these images can be captured in real-time using our projector-camera system, and we encourage the reader to refer to our supplementary materials for video results.

## I. INTRODUCTION

ACTIVE illumination utilizes a controllable light source(s) coupled with detectors to extract meaningful information from the physical world for computer vision and computational photography. These systems range from simple flash photography for better illumination to complex depth and shape acquisition including projector-cameras for structured light [1], active stereo [2], photometric stereo [3], and time-of-flight/LIDAR [4], [5]. Active illumination systems feature a tight integration between hardware and algorithm co-design, and have applications for autonomous vehicles, robotics, and surveillance.

However, most active illumination systems still require strong assumptions regarding the propagation of light from the source to the scene before being captured by the detector. Global light transport effects such as interreflections, scattering, and ambient light can cause depth and shape estimation errors [6]. Further, these illumination systems either inefficient using floodlighting or flashes, or only collect sparse measurements such as in LIDAR. Recently, researchers have proposed new energy-efficient active illumination systems by exploiting the geometry of light paths probed and captured in the scene. These systems utilize the epipolar geometry of the illumination source and detector to capture direct/one-bounce

light, mitigating global light transport effects while capturing accurate depth [7]–[9].

One particular technique for energy-efficient imaging is range or disparity gating. This is where only photons that arrive from a particular depth (range-gating) or surface (disparity-gating) are captured by the detector. In other words, range or disparity gating can capture objects at a certain distance away without capturing other objects or background in the scene at other depths, provided that there is line-of-sight between the sensor and the desired imaging surface. This is particularly useful for imaging through volumetric scattering media such as fog and smoke. Range gating has been implemented using electronic shutters [10] and in coded time-of-flight [11]. Disparity gating has been implemented for planar surfaces (normal to the camera) at certain depths using a synchronized projector-camera system [7], or for arbitrarily curved surfaces at certain depths using a programmable triangulation light curtain [9].

In this paper, we introduce a new technique for disparity gating which obtains photons that arrive from a sloped planar surface of a certain thickness in the scene. We achieve this by controlling the parameters of the rolling shutter of a camera which is synchronized to a raster-scanning projector. This system is a configuration of the Episcan3D [7] where we control the pixel clock, synchronization delay, and camera

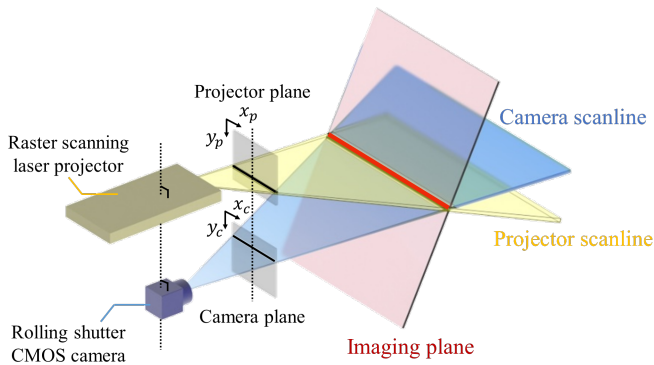


Fig. 2: A visualization of the scanning illumination and the camera rolling shutter performing slope disparity gating.

exposure to perform disparity gating.

Our specific contributions are as follows:

- Capturing sloped planar geometries for disparity gating in real-time using our synchronized projector-camera system.
- Mathematical formulation of the slope geometry and thickness of the gated region as a function of the parameters of rolling shutter pixel clock, synchronization delay between the projection raster and rolling shutter, and exposure of the camera row.
- Applications of sloped disparity gating including real-time image masking and imaging through scattering media.

To validate these ideas in practice, we perform real experiments using a hardware prototype. We hope this paper inspires further research into disparity gating that is energy-efficient and scene geometry-aware in order to maximize the amount of visual information extracted from the world.

## II. RELATED WORK

**Active Illumination Systems:** One of the simplest forms of active illumination for imaging systems is the camera flash for low-light environments. In addition to low-light image enhancement, flash has been generalized to strobing light patterns for high-speed imaging [12]. One of the main applications for active illumination is depth and shape acquisition. Structured light methods have achieved state-of-the-art depth scanning (see comprehensive tutorial [1]). For shape estimation, photometric stereo [3] uses independent light source directions to compute surface normals. New advances in time-of-flight [4] and LIDAR [5] have also enabled ubiquitous depth sensing technology. Active lighting has also helped to improve imaging through scattering media [13], [14], underwater imaging [15], and biomedical microscopy [16].

**Epipolar Imaging:** In this paper, we utilize a projector-camera system based on Episcan3D [7] that performs epipolar imaging. O’Toole *et al.* [7] determined the epipolar geometry of a rectified projector-camera system where projector and

camera rows are both aligned on the same epipolar plane. This also determines which light paths are captured [7], [17], with epipolar light paths containing mostly direct light (i.e. light that only bounces once in a scene), and non-epipolar light paths containing indirect light paths (i.e. light that bounces multiple times in the scene).

Episcan3D synchronizes a laser projector and the rolling shutter of a camera to selectively capture epipolar light when the rolling shutter only exposes camera rows on the same plane as the illuminated projector row, and non-epipolar light when the rolling shutter exposes all camera rows except the row on the same plane as the illuminated projector row [7]. This decomposition of epipolar and non-epipolar light is done in real-time. Further work by Kubo *et al.* [18] showed how Episcan3D can capture indirect light transport, and Achar *et al.* [8] extended epipolar imaging to a time-of-flight camera to obtain more accurate depth measurements and robustness to ambient light.

**Range and Disparity Gating:** Range-gated image sensors utilize synchronized illumination and electronic shutters to only allow light which has traveled a certain time to be exposed by the detector [10], [19]–[21]. These are useful for imaging in scattering media where backscattered light, which reduces contrast in the image, can be optically blocked by gating. Range gating can also be accomplished using time-of-flight cameras [11], [22], [23] or primal-dual coding using synchronized digital micro-mirror devices between projector and camera [24].

Episcan3D performs disparity gating by rotating both the camera and projector 90 degrees, so that the correspondence between projector scanline and camera row becomes dependent on scene disparity or depth (See Section 5.3 of [7]). This captures the equivalent of planar surfaces that are perpendicular to the projector-camera viewpoint, and the synchronization delay controls which range of disparities to gate and capture. This was used to show depth mapping through smoke.

Recently, programmable triangulation light curtains [9] were introduced to perform gated imaging for arbitrary ruled surfaces in 3D. Implemented using a 1D laser illumination synchronized to a 1D line sensor, light curtains can sweep over a surface in 3D and only capture objects that intersect this surface. This is a generalization of disparity gating to an arbitrary surface, and was shown to have robust performance in imaging through scattering media, detecting object intersections with the light curtain, and resilience to strong ambient light.

Our work is a direct extension of Episcan3D’s disparity gating. Our main contribution in this paper is to show how control over the synchronization and hardware parameters for Episcan3D allows the ability to capture sloped planar surfaces for gated imaging. Our system does not have full programmability as does light curtains, but we do have the ability to control the thickness of our sloped planar geometries using exposure, and we can achieve higher frame rates (up to 15 fps) with a dense set of measurements as compared to the scanning 1D illumination and 1D sensor.

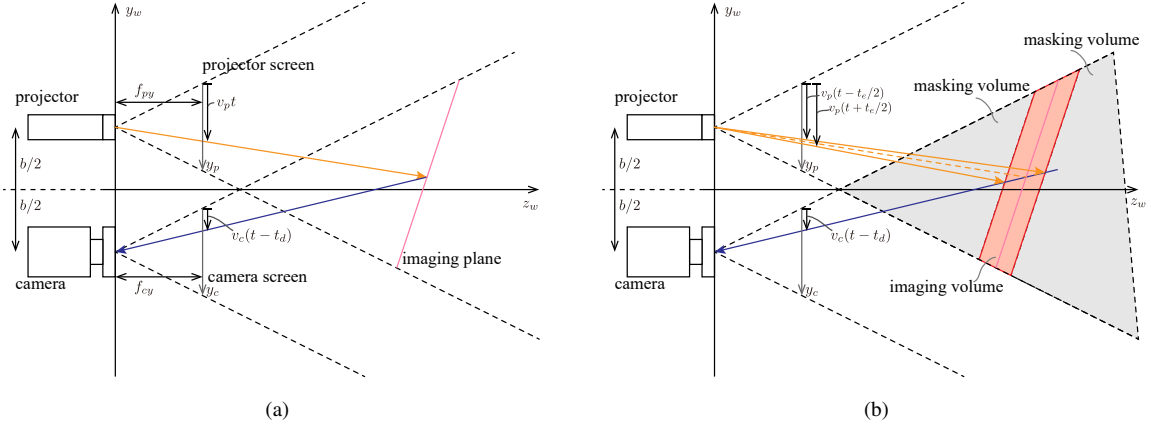


Fig. 3: The ray geometry for our imaging system that determines a sloped plane to be imaged is shown in (a). The effects of exposure allow for volumetric region capture or masking as shown in (b).

### III. GEOMETRY OF SLOPE DISPARITY GATING

In this section, we describe how the parameters of our synchronized projector-camera system, namely delay, exposure, and pixel clock, determine a controllable sloped planar surface in 3D space for gated imaging. We use a laser projector which illuminates a single horizontal plane of the light at a time corresponding to each projector row being illuminated. Our rolling shutter camera captures a single horizontal plane as well corresponding to each exposed pixel row. The illumination plane and camera plane are swept vertically from top row to bottom row, and the projector's optical center is vertically above the camera's origin. A visualization of this projector-camera system is shown in Figure 2.

We thus can formulate the parametric equations for the disparity gated surface as the cross-section between scanning projector and camera planes. We now describe this formulation mathematically in terms of projector-camera geometry. In general, a relation between a position in the world coordinate  $\mathbf{x}_w$  and screen coordinate  $\mathbf{x}_s$  can be described by following equation.

$$s\mathbf{x}_s = \mathbf{K} [\mathbf{R}|\mathbf{T}] \mathbf{x}_w \quad (1)$$

Note,  $\mathbf{x}_s = (x_s, y_s, 1)^\top$  and  $\mathbf{x}_w = (x_w, y_w, z_w, 1)^\top$  are in homogeneous coordinates,  $s$ ,  $\mathbf{R}$  and  $\mathbf{T}$  represents the scaling factor, rotation matrix, and translation vector respectively.  $\mathbf{K}$  represents a camera matrix:

$$\mathbf{K} = \begin{bmatrix} f_x & 0 & c_x \\ 0 & f_y & c_y \\ 0 & 0 & 1 \end{bmatrix}. \quad (2)$$

Our camera is located at  $(0, -b/2, 0)$  and the projector at  $(0, b/2, 0)$ . Both projector and camera are viewing in the  $+z$  direction. The up direction vectors of both projector and camera are  $(0, 1, 0)$ , satisfying the right-hand rule for our coordinate system. In this configuration, the scale factor  $s$  is  $(1, -1, 1)^\top$ , the rotation matrix of the camera  $\mathbf{R}_c$  and of the projector  $\mathbf{R}_p$  are identity matrices, the camera translation vector  $\mathbf{T}_c = (0, b/2, 0)^\top$ , and the projector translation vector is  $\mathbf{T}_p = (0, -b/2, 0)^\top$ .

Thus, the relations between camera screen coordinates  $\mathbf{x}_c = (x_{cs}, y_{cs}, 1)^\top$  to world coordinates, as well as projector screen coordinates  $\mathbf{x}_p = (x_{ps}, y_{ps}, 1)^\top$  to world coordinates is the following:

$$\begin{bmatrix} -y_c \\ 1 \end{bmatrix} = \begin{bmatrix} f_{cy} & c_{cy} \\ 0 & 1 \end{bmatrix} \begin{bmatrix} 1 & 0 & b/2 \\ 0 & 1 & 0 \end{bmatrix} \begin{bmatrix} y_w \\ z_w \\ 1 \end{bmatrix}, \quad (3)$$

$$\begin{bmatrix} -y_p \\ 1 \end{bmatrix} = \begin{bmatrix} f_{py} & c_{py} \\ 0 & 1 \end{bmatrix} \begin{bmatrix} 1 & 0 & -b/2 \\ 0 & 1 & 0 \end{bmatrix} \begin{bmatrix} y_w \\ z_w \\ 1 \end{bmatrix} \quad (4)$$

Since the equations are in homogeneous coordinates, we obtain

$$y_c = -\frac{f_{cy}(y_w + b/2)}{z_w} - c_{cy}, \quad (5)$$

$$y_p = -\frac{f_{py}(y_w - b/2)}{z_w} - c_{py}. \quad (6)$$

Note, we omit  $x$  coordinate in Equations (3)–(6) as the system cannot triangulate with respect to that coordinate axis. We note that this is a limitation of our projector-camera geometry, while programmable light curtains [9] can triangulate any arbitrary curved surface in 3D space.

For arbitrary time  $t$ , the illumination projector row for the scanning projector is given by

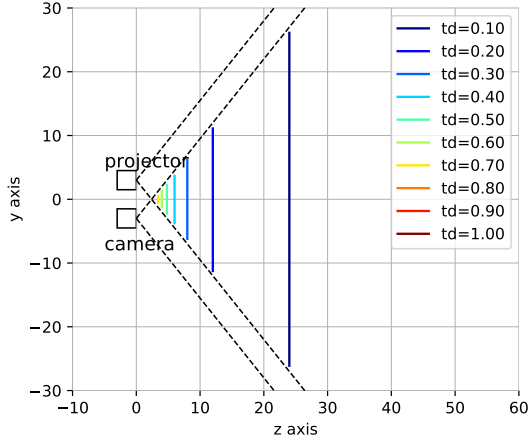
$$y_p = v_p t, \quad (7)$$

and the captured camera row in the rolling shutter is

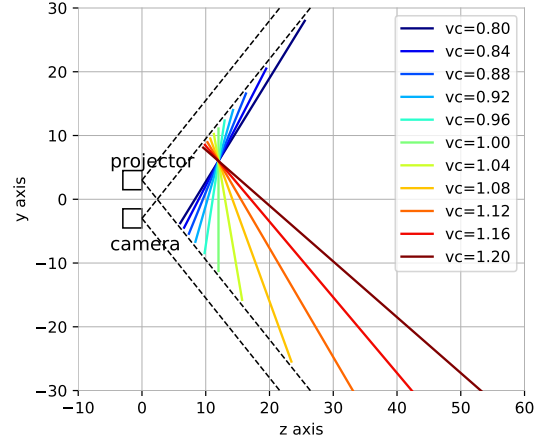
$$y_c = v_c(t - t_d), \quad (8)$$

where  $v_p$  is the projector scanning velocity per row,  $v_c$  is the speed of the rolling shutter per row, and  $t_d$  is the synchronization delay. For now, we do not consider exposure  $t_e$ , although we will later derive the same results with exposure for the general formula.

Since both an illumination row, Equation (7), and a camera row, Equation (8), are in projector and camera screen coordinates, these rows can be converted to world coordinates using



(a) Sweeping delay  $t_d$  from 0.1 to 0.5. Other parameters:  $f_{cy} = f_{py} = 0.8$ ,  $v_c = 1.0$ .



(b) Sweeping camera pixel clock  $v_c$  from  $-1.0$  to  $0.0$ . Other parameters:  $f_{cy} = f_{py} = 0.8$ ,  $t_d = -0.2$ .

Fig. 4: Simulations of the gated imaging plane for different delays  $t_d$  (a) and camera pixel clock  $v_c$  (b).

Equation (6). The intersection of illumination and observation rows in world coordinate can be calculated as

$$y_w = \frac{b(c_{cy}f_{py} + c_{py}f_{cy} + f_{py}v_c(t - t_d) + f_{cy}v_p t)}{2(c_{cy}f_{py} - c_{py}f_{cy} + f_{py}v_c(t - t_d) - f_{cy}v_p t)}, \quad (9)$$

$$z_w = \frac{-bf_{cy}f_{py}}{c_{cy}f_{py} - c_{py}f_{cy} + f_{py}v_c(t - t_d) - f_{cy}v_p t}. \quad (10)$$

These equations represent a single sloped plane in  $y-z$  world coordinates parameterized by  $t$ . In Figure 3(a), we visually depict this sloped plane that is triangulated by the projector and camera planes. Note that this surface is defined by parameters of the system including synchronized delay  $t_d$ , rolling shutter velocity of the camera  $v_c$ , and the projector scanning velocity  $v_p$ . This is the surface that we are performing gated imaging on.

Our synchronized projector-camera system only obtains the direct reflection component or first bounce light on the surface unless the second or higher-order bounce components are weak enough. Since both the distance  $z$  and slope of the plane can be controlled by our system, we title our imaging method *slope disparity gating*.

**Camera Exposure:** In the previous equations, we did not consider the effects of camera exposure  $t_e$  on this gated plane. For arbitrary time  $t$ , a camera row  $y_{cs}$  and  $y_{ce}$  that starts and ends the exposure, respectively, can be calculated as

$$y_{cs} = v_c \left( t - t_d - \frac{t_e}{2} \right) \quad (11)$$

$$y_{ce} = v_c \left( t - t_d + \frac{t_e}{2} \right), \quad (12)$$

in camera screen coordinates. When computing the swept cross-section between the illumination and camera planes, the finite exposure causes the cross-section to become a 3D volume as shown in Figure 3(b). This allows us to change the thickness of this volume solely based on the camera exposure. This is a fundamentally novel feature of our projector-camera system as compared to programmable light curtains [9] which

requires a physical change in either the baseline or optics of the system to control the thickness of the light curtains.

#### Rolling Shutter Pixel Clock and Synchronization Delay:

A key insight into our system is that the camera's rolling shutter pixel clock controls the scanning velocity of the camera. By changing the pixel clock, we can change  $v_c$ , and control the slope of the triangulated surface as shown in Figure 4(b). By changing the value of the delay  $t_d$ , the distance to the sloped surface can be controlled shown in Figure 4(a) similar to the configuration described in [7]. One disadvantage of our hardware implementation is that we cannot control the projector's sweeping velocity, thus, we fix  $v_p$  in our simulations.

In Figure 5, we show the timing diagram of our system with respect to the conventional Episcan3D disparity gating. Note that with the projector and camera velocities synchronized in (a), this corresponds to a vertical gated region. However, changing the pixel clock as discussed earlier will result in the timing diagram (b), which corresponds to sloped gated regions that are captured.

#### IV. HARDWARE IMPLEMENTATION

**Setup:** Our experimental prototype is similar to the Episcan3D system configured in disparity gating mode [7]. This involves a laser projector and a rolling shutter camera that are synchronized to one another. We use a SONY MP-CL1A laser projector with  $1280 \times 720$  resolution and a 60Hz refresh rate. We use either an IDS UI-3250CP-C-HQ color camera or IDS UI-3250CP-M-GL monochrome camera with both global and rolling shutter capabilities. We utilize two cameras: a main camera that is synchronized to the projector, and a helper camera for help with capturing regular images although it is not necessary for the proposed system. We set the main camera to the rolling shutter mode and set the helper camera to global shutter mode.

Figure 6 shows the system configuration we actually implemented. Using a model shaped by 3D printing, we aligned vertically the optical axes of the laser projector

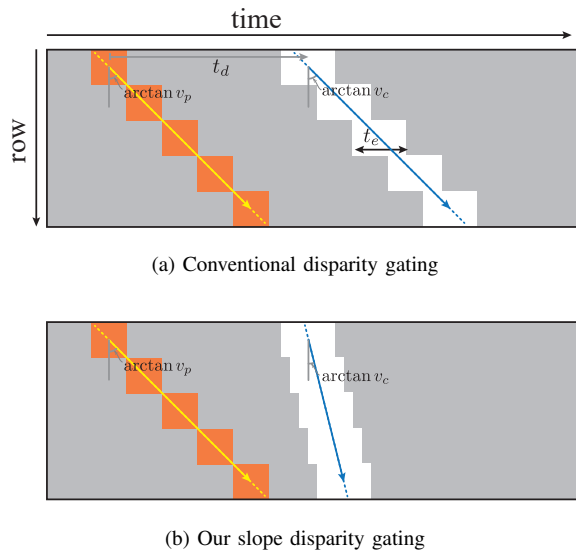


Fig. 5: Timing diagram of projector illumination and camera rolling shutter for conventional Episcan3D with the same projector and camera velocities (a) and for our system with a different camera velocity that causes the sloped planar region for disparity gating (b).

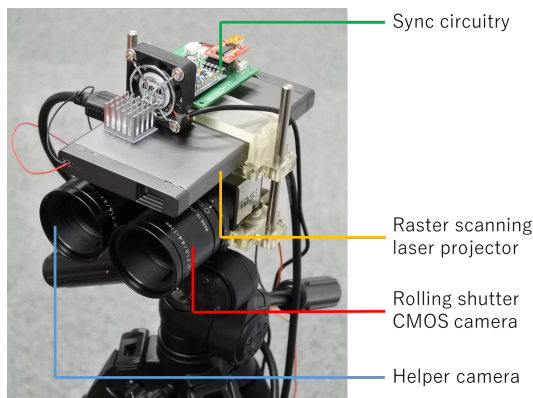


Fig. 6: Our hardware prototype consisting of vertically-aligned projector-camera with synchronization electronics.

and a rolling shutter camera. The main camera triggers the rolling shutter using the vertical scanning signal of the projector as the trigger signal. We refer the reader to the supplemental material of [7] for further information about the synchronization circuitry. We use a band-pass filter of 640nm in front of the main monochrome camera sensor to reduce ambient light contributions.

**Acquisition:** We used 12 bit capture for each captured image. The range of pixel clock frequencies allowable by our hardware is 10–50MHz with increments of 1MHz, 50–100MHz with increments of 2MHz, and 100–128MHz with increments of 4MHz. We are able to capture a single image in real-time using our hardware prototype.

In this section, we present results from our experimental prototype performing slope disparity gating. The main application for this imaging technique is imaging through scattering media.

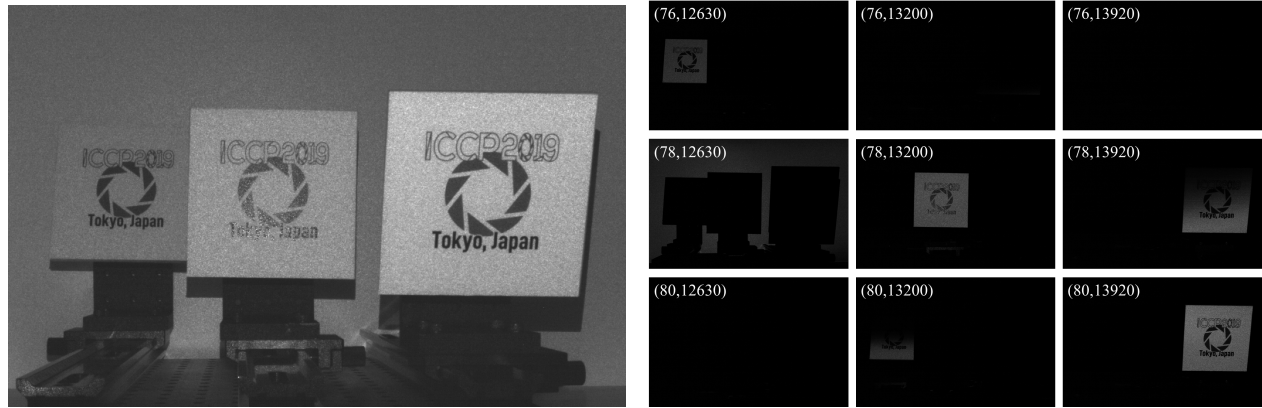
**Slope Disparity Gating:** In Figure 7, we show a demonstration of slope disparity gating to selectively image portions of the scene. In the scene shown in Figure 7 (a), we display three different planar targets, tilted at  $+15, 0, -15$  degrees and spaced 15cm apart. Using pixel clocks of 76, 78, 80MHz and delays 12630, 13200, 13920 $\mu$ s, we can selectively image the three planar targets in Figure 7 (b). Please refer to the supplemental material for a video imaging this scene. Experimentally, we even can image the planar targets of  $+75$  degrees using a pixel clock of 50MHz, and  $-75$  degrees using a pixel clock of 108MHz.

In addition to selectively gating targets, we can also mask regions in the scene in Figure 7 (c) where all the targets are tilted at  $+15$  degrees. We show that we can selectively mask the planar targets with different delay and exposure values in Figure 7 (d–f). We note that we calculate and implement the parameter values for the masking manually, and it remains an area of future work to determine an object’s position and slope in a scene and automatically set the delay, exposure, and pixel clock for gated imaging and/or masking.

In the teaser Figure 1, we show the effect of using pixel clock to slope our disparity gating region to perform either imaging or masking. Here, the table with the document is either imaged or selectively masked. For real-time video of this image masking, please refer to the supplementary material. This image masking is useful for security applications since it is a hardware solution that discards photons before it even reaches the sensor, similar to other privacy-preserving optics solutions [25].

Both disparity gating and masking can be performed in real-time by setting the appropriate pixel clock, exposure, and synchronization delay. However, due to limitations of the current hardware, we cannot perform dynamic image gating where we can change the gated region being imaged or masked in real-time. This is because the current camera API does not allow us to change the pixel clock, delay, or exposure without interrupting streaming frames. It remains an avenue of future work to dynamically change the size or shape of the gated region in real-time.

One application of the Episcan3D system is its ability to image veins in the skin using visible light. This can be done using an appropriate delay to capture the short-range indirect light scattered by the vein structures. Slope disparity gating gives us an additional degree of control for these vein images. In Figure 8, we see two arms with different vertical slopes in (a) and (d). Note how by changing the pixel clock, we are able to selectively image the veins in the arm at different orientations in (c) and (e). This shows the importance of pixel clock to adjust the disparity gating for off-axis limbs. A limitation of this experiment is that the arm can only slope in the vertical direction, as horizontal disparity gating is not



(a) Regular image

(b) Acquired images of each pixel clock and delay



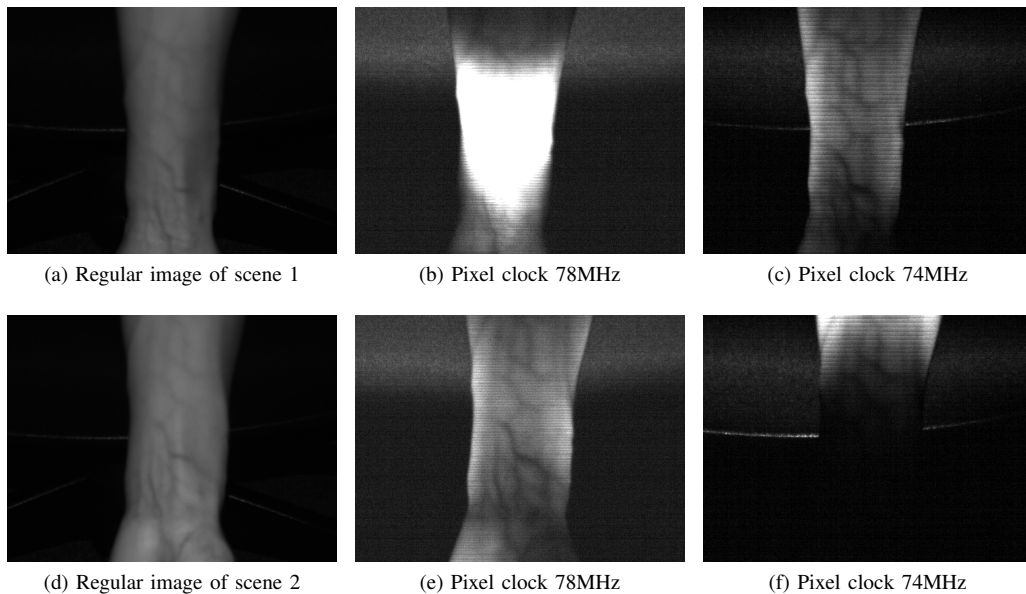
(c) Regular image

(d)  $t_d = 12660\mu s, t_e = 600\mu s$

(e)  $t_d = 13090\mu s, t_e = 600\mu s$

(f)  $t_d = 21270\mu s, t_e = 16400\mu s$

Fig. 7: Slope disparity gating results: (a) Planar targets oriented at  $+15, 0, -15$  degrees and 15cm apart. (b) Selective imaging of these targets using different pixel clock and delay, denoted in the upper left as  $(v_c, t_d)$ . (c) Planar targets  $+15$  degrees oriented. (d)–(f) Selectively masking each planar target by changing delay and exposure to control the thickness and placement of the volumetric gated region. Each image was an average of 10 frames for visualization enhancement. Please refer to the supplementary material for video results.



(a) Regular image of scene 1

(b) Pixel clock 78MHz

(c) Pixel clock 74MHz

(d) Regular image of scene 2

(e) Pixel clock 78MHz

(f) Pixel clock 74MHz

Fig. 8: Capturing short range indirect light to visualize human veins requires an appropriate pixel clock. We tested two scenes of tilted arms with different angles. Each image was an average of 10 frames for enhanced visualization in this figure. For an arm shown in (a), the veins of the arm are more visible with a pixel clock of 74 MHz shown in (c) as compared to (b) with pixel clock of 78 MHz. For another arm oriented differently in (d), image (e) with pixel clock of 78 MHz is more visible than in image (f) with pixel clock of 74 MHz. Since conventional disparity gating cannot change the pixel clock, only our system can perform this imaging for different vertically sloped arms.

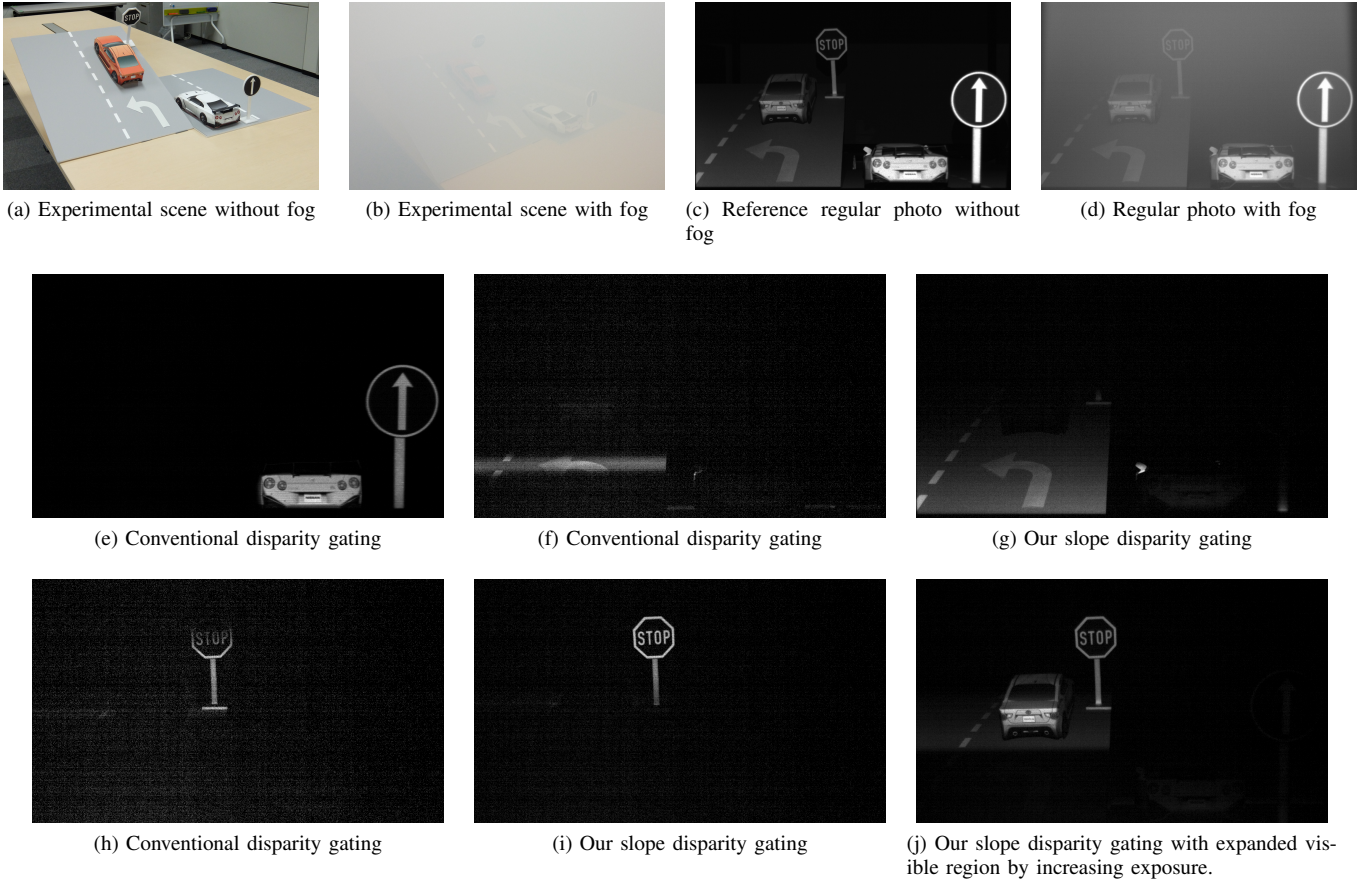


Fig. 9: Experimental results in fog scene. We built a miniature scene emulating a traffic scene (a) with artificially-generated fog (b). Compared to a regular photo without fog (c), the captured image in fog (d) decreases the contrast and visibility for regular cameras. Conventional disparity gating [7] can significantly enhance the visibility of the objects on the same vertical plane (e), but can not visualize tilted surfaces (f). By controlling the synchronization delay and pixel clock, our device can visualize the entire area of the tilted surface and resolve the arrow sign on the road (g). Similarly, while conventional disparity gating can partially capture the sign on the tilted surface (h), our method can capture the sign entirely (i). Moreover, our device can expand the visible volume by increasing exposure time as shown in (j). Each image in this figure was an average of 5 frames to improve the visualization. Please refer to the supplementary material for a visualization of the results for imaging through fog.

possible with our hardware configuration.

**Imaging through Scattering Media:** One of the main applications of disparity gating is imaging through scattering media. This has applications for imaging through bad weather like fog and rain [26] and underwater imaging [13]. Using disparity gating, we can improve imaging through scattering media by selectively capturing only photons from the region of interest. In Figure 9 (a), we image a small scene that emulates cars driving on a road. We use a ROSCO Alpha 900 v2 fog machine that uses water vapor to generate fog that reduces the visibility of the camera (as shown in Figure 9 (b)). In Figure 9 (c) and (d), we see the effects of capturing the scene with and without fog present using a regular camera. In Figure 9 (e) and (f), we perform conventional disparity gating to capture either the car in front or a portion of the turn symbol on the road. Note that the vertical geometry of the gated region limits how much scene is captured. In contrast, our method of slope disparity gating shown in Figure 9 (g)

captures the full turn symbol by utilizing a sloped planar region to capture the arrow. In Figure 9 (h), we see that conventional disparity gating can resolve the stop sign, but there is still issue with less visible on upper region because the sign is placed on the sloped road. In contrast, our slope disparity gating can resolve the stop sign in Figure 9 (i), and we can expand the volumetric region where we image to see more context in Figure 9 (j). We believe this scene shows the versatility of slope disparity gating for imaging through scattering media. For video results, we encourage the reader to please view the supplementary material for imaging through fog.

## VI. DISCUSSION

In this work, we have demonstrated an active illumination system that is able to perform gated imaging controllable for planes sloped in the  $y$ - $z$  plane. This system was implemented using the pixel clock, synchronization delay, and exposure for a vertically-aligned configuration of the Episcan3D system [7].

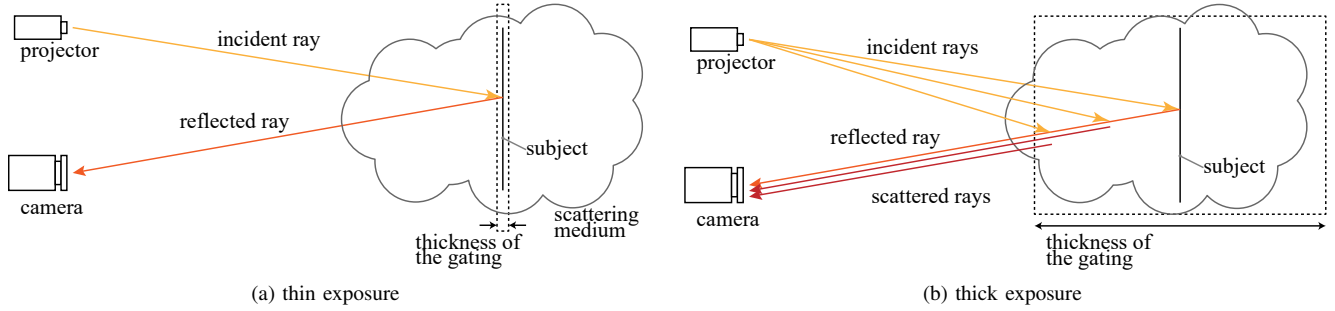
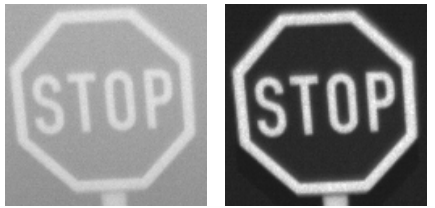
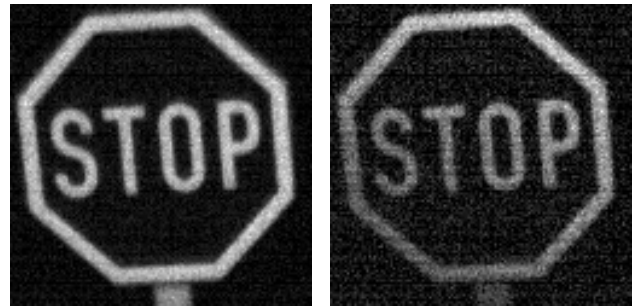


Fig. 10: To capture an object in scattering media such as fog, a tight exposure will capture only reflected ray from the object (a). A larger exposure can extend the visible region, however, this results in capturing more scattered light. The intensity of the scattered light increases linearly along the thickness of the gating assuming single scattering is dominant and there is no scattering extinction coefficient.



(a) Regular with fog (b) Reference regular without fog

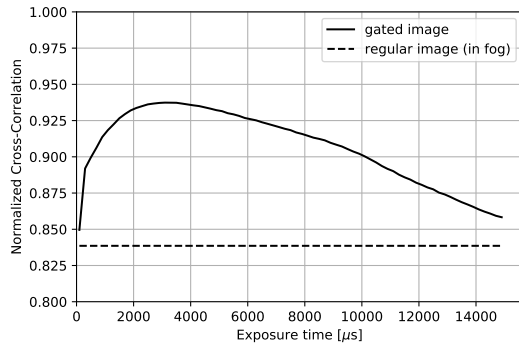


(a)  $t_e = 300\mu s$  (b)  $t_e = 100\mu s$



(c)  $t_e = 300\mu s$  (d)  $t_e = 3500\mu s$  (e)  $t_e = 7500\mu s$

Fig. 12: Exposure time vs. SNR. As we can see, smaller exposure time leads to higher noise in (b) due to the less light arriving at the sensor from the thin gated region. Each image was averaged over 5 frames to enhance visualization.



(f)

Fig. 11: Exposure time vs. Normalized Cross-Correlation (NCC). (a) – (e) The displayed signs are cropped from the same scene in Figure 9. (a) Regular image in fog. (b) Regular image without fog as a reference. (c) – (e) The gated images acquired for varying exposure time  $t_e$  while fixing delay  $t_d = 12980$  to image the stop sign. (f) The NCC of each image compared to (b), sweeping  $t_e = 300 \sim 14900\mu s$ . Each image was averaged over 5 frames to enhance visualization.

We demonstrated applications of this system including real-time image masking as well as imaging through scattering media.

In disparity gating, there is a trade-off between the exposure and the contrast of the captured imaging. In Figure 10, we see that when the exposure is small resulting in a thin gated region, a smaller amount of backscattered light is captured, resulting in fewer objects imaged in the scene. However, when the exposure is large resulting in a thick gated region encompassing the scattering media, incident rays from the projector get backscattered into the camera detector, reducing the contrast of the captured image. In Figure 11, we empirically show this reduced normalized cross-correlation (NCC) as a function of exposure time, sweeping exposure time from  $300\mu s - 14,000\mu s$ . In addition, in Figure 12, we see that using a short exposure requires in higher noise values, as the volume of the gated region becomes thinner and thus less light is captured by the sensor. This trade-off between exposure, NCC, SNR, and gated region size is an interesting design point for future range and disparity gating systems.

**Comparison to Related Work:** Our slope disparity gating technique extends the disparity gating configuration of

Episcan3D in [7] to handle sloped planar geometries as well as control the volume of the gated region using the exposure of the camera. However, there is a limited set of limited geometries we can perform gated imaging as compared to programmable light curtains [9] which can triangulate any arbitrary ruled surface in 3D. However, we are able to perform imaging slightly faster (15 fps) as compared to light curtains (5.6 fps), and we can control the thickness of our gated region more easily than light curtains which needs to adjust either the baseline, focal length, or laser thickness to achieve the same effect. Finally, although we do not utilize it in our paper, we are able to easily project patterns in the disparity images which may be an interesting avenue for future work with structured light algorithms.

**Limitations:** There are several limitations to our imaging system proposed here. These include a coarse control over the pixel clock (with 1, 2, and 4 MHz increments) and a fixed projector scanning rate due to hardware limitations. As noted earlier, our system cannot perform arbitrary surface or volumetric gated imaging, which limits its application domains and scenes where it can perform selective imaging/masking.

**Future Work:** Future work involves using visual features in the scene to determine the optimal pixel clock, delay, and exposure to capture salient objects within the gated imaging region. This could include changing the slope of the disparity gating dynamically as an object moves in a tight feedback loop. In addition, it would be useful to apply techniques such as coded or patterned projector and rolling shutter scanning to selectively encode and parse the light transport paths captured in the scene.

#### ACKNOWLEDGMENT

This work was sponsored by the JSPS KAKENHI grant number JP15K16027 and JST CREST JPMJCR1764.

#### REFERENCES

[1] J. Geng, "Structured-light 3d surface imaging: a tutorial," *Advances in Optics and Photonics*, vol. 3, no. 2, pp. 128–160, Jun 2011. [Online]. Available: <http://aop.osa.org/abstract.cfm?URI=aop-3-2-128>

[2] C. Je, S. W. Lee, and R.-H. Park, "High-contrast color-stripe pattern for rapid structured-light range imaging," in *European Conference on Computer Vision*. Springer, 2004, pp. 95–107.

[3] R. J. Woodham, "Photometric method for determining surface orientation from multiple images," *Optical Engineering*, vol. 19, no. 1, p. 191139, 1980.

[4] S. B. Gokturk, H. Yalcin, and C. Bamji, "A time-of-flight depth sensor-system description, issues and solutions," in *Computer Vision and Pattern Recognition Workshop, 2004. CVPRW'04. Conference on*. IEEE, 2004, pp. 35–35.

[5] B. Schwarz, "Lidar: Mapping the world in 3d," *Nature Photonics*, vol. 4, no. 7, p. 429, 2010.

[6] M. Gupta, A. Agrawal, A. Veeraraghavan, and S. G. Narasimhan, "A practical approach to 3d scanning in the presence of interreflections, subsurface scattering and defocus," *International Journal of Computer Vision*, vol. 102, no. 1-3, pp. 33–55, 2013.

[7] M. O'Toole, S. Achar, S. G. Narasimhan, and K. N. Kutulakos, "Homogeneous codes for energy-efficient illumination and imaging," *ACM Transactions on Graphics*, vol. 34, no. 4, pp. 35:1–35:13, Jul. 2015. [Online]. Available: <http://doi.acm.org/10.1145/2766897>

[8] S. Achar, J. R. Bartels, W. L. Whittaker, K. N. Kutulakos, and S. G. Narasimhan, "Epipolar time-of-flight imaging," *ACM Transactions on Graphics*, vol. 36, no. 4, p. 37, 2017.

[9] J. Wang, J. Bartels, W. Whittaker, A. C. Sankaranarayanan, and S. G. Narasimhan, "Programmable triangulation light curtains," in *The European Conference on Computer Vision (ECCV)*, September 2018.

[10] O. David, N. S. Kopeika, and B. Weizer, "Range gated active night vision system for automobiles," *Applied Optics*, vol. 45, no. 28, pp. 7248–7254, 2006.

[11] A. Kadambi, R. Whyte, A. Bhandari, L. Streeter, C. Barsi, A. Dorrington, and R. Raskar, "Coded time of flight cameras: sparse deconvolution to address multipath interference and recover time profiles," *ACM Transactions on Graphics*, vol. 32, no. 6, p. 167, 2013.

[12] H. E. Edgerton and J. R. Killian, *Flash!: Seeing the unseen by ultra high-speed photography*. Hale, Cushman & Flint, 1939.

[13] M. Gupta, S. G. Narasimhan, and Y. Y. Schechner, "On controlling light transport in poor visibility environments," in *IEEE Conference on Computer Vision and Pattern Recognition (CVPR)*. IEEE, 2008, pp. 1–8.

[14] S. G. Narasimhan, S. K. Nayar, B. Sun, and S. J. Koppal, "Structured light in scattering media," in *IEEE International Conference on Computer Vision (ICCV)*, vol. 1. IEEE, 2005, pp. 420–427.

[15] T. Treibitz and Y. Y. Schechner, "Active polarization descattering," *IEEE Transactions on Pattern Analysis and Machine Intelligence*, no. 3, pp. 385–399, 2008.

[16] L. Tian, X. Li, K. Ramchandran, and L. Waller, "Multiplexed coded illumination for fourier ptychography with an led array microscope," *Biomedical Optics Express*, vol. 5, no. 7, pp. 2376–2389, 2014.

[17] M. O'Toole, J. Mather, and K. N. Kutulakos, "3d shape and indirect appearance by structured light transport," in *IEEE Conference on Computer Vision and Pattern Recognition (CVPR)*, 2014, pp. 3246–3253.

[18] H. Kubo, S. Jayasuriya, T. Iwaguchi, T. Funatomi, Y. Mukaigawa, and S. G. Narasimhan, "Acquiring and characterizing plane-to-ray indirect light transport," in *IEEE International Conference on Computational Photography (ICCP)*, May 2018, pp. 1–10.

[19] I. Baker, S. S. Duncan, and J. W. Copley, "A low noise, laser-gated imaging system for long range target identification," *Proceedings of SPIE - The International Society for Optical Engineering*, vol. 5406, 08 2004.

[20] Y. Grauer and E. Sonn, "Active gated imaging for automotive safety applications," in *Video Surveillance and Transportation Imaging Applications 2015*, vol. 9407. International Society for Optics and Photonics, 2015, p. 94070F.

[21] D. Bonnier and V. Laroche, "Range-gated active-imaging system for search-and-rescue and surveillance operations," in *Infrared Technology and Applications XXII*, vol. 2744. International Society for Optics and Photonics, 1996, pp. 134–146.

[22] F. Heide, M. B. Hullin, J. Gregson, and W. Heidrich, "Low-budget transient imaging using photonic mixer devices," *ACM Transactions on Graphics*, vol. 32, no. 4, p. 45, 2013.

[23] R. Tadano, A. Kumar Pediredla, and A. Veeraraghavan, "Depth selective camera: A direct, on-chip, programmable technique for depth selectivity in photography," in *IEEE International Conference on Computer Vision (ICCV)*, 2015, pp. 3595–3603.

[24] M. O'Toole, R. Raskar, and K. N. Kutulakos, "Primal-dual coding to probe light transport," *ACM Transactions on Graphics*, vol. 31, no. 4, pp. 1–11, 2012. [Online]. Available: <http://dl.acm.org/citation.cfm?doi=2185520.2185535>

[25] F. Pittaluga and S. J. Koppal, "Pre-capture privacy for small vision sensors," *IEEE Transactions on Pattern Analysis and Machine Intelligence*, vol. 39, no. 11, pp. 2215–2226, 2017.

[26] S. K. Nayar and S. G. Narasimhan, "Vision in bad weather," in *IEEE International Conference on Computer Vision*, vol. 2. IEEE, 1999, pp. 820–827.